AIP | Physics of Fluids

Viscous fluid injection into a confined channel

Zhong Zheng, Laurence Rongy, and Howard A. Stone

Citation: Physics of Fluids **27**, 062105 (2015); doi: 10.1063/1.4922736
View online: http://dx.doi.org/10.1063/1.4922736
View Table of Contents: http://scitation.aip.org/content/aip/journal/pof2/27/6?ver=pdfcov
Published by the AIP Publishing

PHYSICS OF FLUIDS **27**, 062105 (2015)

Viscous fluid injection into a confined channel

Zhong Zheng,[1] Laurence Rongy,[2] and Howard A. Stone[1,a)]
[1]*Department of Mechanical and Aerospace Engineering, Princeton University, Princeton, New Jersey 08544, USA*
[2]*Nonlinear Physical Chemistry Unit, Faculté des Sciences, Université libre de Bruxelles (ULB), CP231, 1050 Brussels, Belgium*

(Received 27 January 2015; accepted 8 June 2015; published online 22 June 2015)

We analyze the injection of a viscous fluid into a two-dimensional horizontal confined channel initially filled with another viscous fluid of different density and viscosity. We study the flow using the lubrication approximation and assume that the mixing between the fluids and their interfacial tension are negligible. When the injection rate is maintained constant, the evolution of the fluid-fluid interface can be described by a nonlinear advection-diffusion equation dependent only on the viscosity ratio between the two fluids. In the early time period, the advection-diffusion equation reduces to a well-known nonlinear diffusion equation, and a self-similar solution is obtained. In the late time period, the advection-diffusion equation is approximated by a nonlinear hyperbolic equation, and a compound wave solution is constructed to describe the time evolution of the fluid-fluid interface. Numerical solutions of the full equation show good agreement with the analytical solutions in both the early and late time periods. Finally, a regime diagram is obtained to summarize the flow behaviours with regard to two dimensionless groups: the viscosity ratio of the two fluids and the dimensionless time; three different dynamical behaviours are identified in the regime diagram: a nonlinear diffusion regime, a hyperbolic regime, and a transition regime. This problem is analogous to the corresponding injection flow problem into a confined porous medium. © *2015 AIP Publishing LLC.* [http://dx.doi.org/10.1063/1.4922736]

I. INTRODUCTION

The filling or cleaning of channels generally requires the displacement of the original liquid by a second fluid. The time evolution of such two-phase viscous displacement processes involves both buoyancy effects, when the two liquids have different densities, and the rate of injection of the second fluid. We investigate these displacement processes using a formalism familiar from the literature on viscous gravity currents and highlight the impact of geometric confinement.

For the case of fluid injection into a confined channel, and at times short enough that the injected fluid does not attach to the second boundary, this problem is well-approximated by the spreading of a viscous gravity current on a horizontal plane where the spreading volume increases linearly in time. At late times, the injected fluid reaches the second boundary and the solution is best described as a compound wave solution, whose structure is determined in this paper.

Many of the features we discuss are related to themes in the literature on gravity currents, which occur whenever horizontal density gradients exist in a gravity field, with the denser fluid naturally sinking below the less dense fluid. The propagation of viscous gravity currents, when the inertial effects can be neglected, has been studied extensively due to its relevance in a wide range of geophysical and industrial contexts.[1–5] Typically, in unconfined geometries, the propagation of a viscous gravity current has been studied without considering the motion of the ambient fluid. In the absence of surface tension effects, the system of equations, written in the lubrication approximation, reduces to a second-order nonlinear partial differential equation in space and time for the thickness

[a)]Electronic mail: hastone@princeton.edu.

TABLE I. Summary of typical flow situations in confined geometries (confined porous media or channels) when the propagation of a viscous gravity current exhibits a transition from an early time self-similar solution to a distinct late time self-similar solution. The transition of the propagation law for the moving fronts are included in this table with x representing the length of the current and t representing time.

Initial condition	Flow constraints	Early time	Late time	References
Post-injection, confined shape	Constant volume, porous media	$x \propto t^{1/2}$	$x \propto t^{1/3}$	Hesse *et al.*[19]
Lock exchange, step function	Constant volume, Hele-Shaw cells	$x \propto t$	$x \propto t^{1/2}$ $x \propto t^{1/3}$ $x \propto t^{1/5}$	Hallez and Magnaudet[20]
Point source, no injected fluid	Constant injection, porous media	$x \propto t^{2/3}$	$x \propto t$	Pegler *et al.*[21] Zheng *et al.*[22]
Lock exchange, step function	Constant injection, wide channel	$x \propto t^{1/2}$	$x \propto t$	Taghavi *et al.*[23]
Point source, no injected fluid	Constant injection, wide channel	$x \propto t^{4/5}$	$x \propto t$	Current work

of the current. This equation was derived in the case of a viscous gravity current flowing along a horizontal wall,[6–9] down a slope,[10,11] and in a porous medium.[1,2,12–16] When the injected volume is proportional to a power of time, various similarity solutions have been obtained and compared with experimental results. The influence of heterogeneity has also been studied using both models and laboratory-scale experiments in V-shaped channels of varying gap thickness in the vertical direction[17,18] and horizontal direction.[16]

The propagation of viscous gravity currents in confined porous media has received more research interest recently. For fluid injection into a confined porous medium with near horizontal boundaries, in the limit of the lubrication approximation, the motions of both the injected and displaced fluids are considered, and a nonlinear advection-diffusion equation is obtained for the propagation of a gravity current.[1,12,19,21,22,24–28]

In confined geometries, a significant feature is that there is a time when the fluid flow transitions between the unconfined and confined behaviours. The two-layer gravity current created by the release of a finite volume of one fluid into a porous medium saturated with another fluid with different density and viscosity was investigated by Hesse *et al.*,[19] and they show that there exists a transition from an early time self-similar solution to a distinct late time self-similar solution that is independent of the viscosity ratio. Also, the study of constant fluid injection into a horizontal confined porous medium reveals a transition from an early time nonlinear diffusion behaviour to three distinct late time self-similar behaviours depending on the viscosity ratio of the two fluids.[21,22] The viscous lock exchange flows in a two-dimensional horizontal confined channel have also been investigated, and different flow behaviours have been observed in the early and late time periods.[23,29,30] Table I summarizes some typical situations in a confined geometry, including channels and porous media, when the propagation of a viscous gravity current exhibits a transition from an early time self-similar solution to another late time self-similar solution.

The purpose of this paper is to analyze the injection of a viscous fluid into a two-dimensional horizontal confined channel initially filled with another fluid of different density and viscosity. This configuration is common to many filling, cleaning, or fluid replacement operations; we show that this problem contributes to another situation when the early and late time flow behaviours exhibit different self-similar solutions, see Table I. We introduce in Sec. II the model that describes the resulting two-layer gravity current with the incompressible form of Stokes equations approximated within the lubrication limit. In this case, following standard steps, the vertical pressure gradient is hydrostatic, the equations can be integrated analytically, and the dynamics of the gravity current can be described by a single nonlinear partial differential equation. We show in Sec. III that in the early time period, the dynamics of the interface can be described by a nonlinear diffusion equation and recover the self-similar solution describing a gravity current in a unconfined channel. In Sec. IV, we study the late time dynamics of the fluid-fluid interface and a compound wave solution is obtained. The transition process from the early time to late time behaviours is discussed in Sec. V by numerically tracking the propagation laws of the moving front. Finally, a regime diagram is obtained to summarize the flow behaviours with regard to two dimensionless groups: the viscosity ratio and

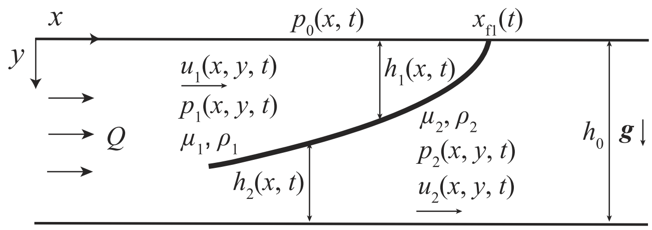

FIG. 1. Sketch of the system. Viscous exchange flow with constant fluid injection in a horizontal channel with depth h_0 and infinite length. The injected and displaced fluids are immiscible and separated by a sharp interface with a propagating front $x_{f1}(t)$. The fluids have different viscosities, and for the sketch in this figure, the injected fluid is less dense than the displaced fluid.

the dimensionless time. We conclude our paper in Sec. VI by summarizing the major findings and discussing the connections with previous studies.

II. THEORETICAL MODEL

We consider a two-layer viscous gravity current in a two-dimensional horizontal confined channel of constant height h_0; inertial effects are neglected. The channel width into the page is assumed much larger than h_0 and so we model the flow as two-dimensional. The injected fluid is denoted 1 and the displaced fluid, 2. Typically, the two fluids have different viscosities, μ_1 and μ_2, and different densities, ρ_1 and ρ_2, so that the denser fluid sinks below the other one (see Figure 1). We define $\lambda \equiv \mu_2/\mu_1$, the viscosity ratio between the two fluids; we also define $\Delta\rho \equiv \rho_2 - \rho_1$, the density difference of the two fluids. We study the case when one fluid is injected at a constant flow rate q, which imposes an additional pressure gradient for the fluid motion. The dynamics of the problem consist of an interplay, mediated by confinement, of the effects of injection and buoyancy-driven flow. We assume the injected fluid is less dense than the displaced fluid, i.e., $\Delta\rho > 0$; a similar analysis applies to the case with $\Delta\rho < 0$, i.e., when the injected fluid is denser than the displaced fluid.

We assume that the mixing between the two fluids can be neglected and also neglect the effects of surface tension at the fluid-fluid interface. We denote x and y as, respectively, the horizontal and vertical coordinates, with y measured positive downward. Thus, there is a sharp interface $y = h_1(x,t)$ between the two fluids (Figure 1); determining the time evolution of the interface $h_1(x,t)$ is the focus of this paper. In the limit where the current length is much greater than its depth, the flow is primarily horizontal and the vertical velocity is negligible. Then, the pressures in the fluids have a hydrostatic distribution:

$$p_1(x,y,t) = p_0(x,t) + \rho_1 g y, \quad \text{for } 0 \le y \le h_1(x,t), \tag{1a}$$

$$p_2(x,y,t) = p_0(x,t) + \rho_1 g h_1(x,t) + \rho_2 g(y - h_1(x,t)), \quad \text{for } h_1(x,t) \le y \le h_0, \tag{1b}$$

where $p_1(x,y,t)$ and $p_2(x,y,t)$ denote, respectively, the pressures in the injected and displaced fluids, and $p_0(x,t)$ represents the pressure at the impermeable top boundary. We note that given the hydrostatic pressure distribution (1), the pressure gradients $p_{1x} \equiv \partial p_1/\partial x$ and $p_{2x} \equiv \partial p_2/\partial x$ are independent of y.

The fluid motion is governed by a balance between pressure gradients and viscous forces and can be described by the Stokes equation simplified by the lubrication approximation,

$$\frac{\partial p_1}{\partial x} = \mu_1 \frac{\partial^2 u_1}{\partial y^2}, \tag{2a}$$

$$\frac{\partial p_2}{\partial x} = \mu_2 \frac{\partial^2 u_2}{\partial y^2}, \tag{2b}$$

where $u_1(x,y,t)$ and $u_2(x,y,t)$ denote the horizontal velocities of the injected and displaced fluids, respectively. Note that we have neglected the velocities in the vertical direction based on the lubrication approximation.

The appropriate boundary conditions for Eq. (2) are no-slip for the velocities along the top and bottom horizontal boundaries, and continuity of velocity and tangential stress across the interface between the two fluids,

$$y = 0: \; u_1 = 0, \qquad y = h_1(x,t): \; u_1 = u_2, \tag{3a}$$

and

$$\mu_1 \frac{\partial u_1}{\partial y} = \mu_2 \frac{\partial u_2}{\partial y}, \tag{3b}$$

$$y = h_0: \; u_2 = 0. \tag{3c}$$

Equation (2) along with four boundary conditions (3) forms a complete problem statement and can be solved analytically. The horizontal velocities of the fluids are obtained in terms of the pressure gradients,

$$u_1(x,y,t) = \frac{p_{1x}}{2\mu_1}\left\{ y^2 - \frac{[2h_0 + (\lambda-2)h_1]\, h_1 p_{1x} + (h_0-h_1)^2 p_{2x}}{[(\lambda-1)h_1 + h_0]\, p_{1x}}\, y \right\}, \tag{4a}$$

$$u_2(x,y,t) = \frac{p_{2x}}{2\mu_2}\left\{ y^2 + \frac{\lambda h_1^2 p_{1x} - \left(h_0^2 - (1-2\lambda)h_1^2\right) p_{2x}}{[(\lambda-1)h_1 + h_0]\, p_{2x}}\, y - \frac{\lambda h_0 h_1^2 p_{1x} + h_0 h_1 [(\lambda-1)h_0 + (1-2\lambda)h_1]\, p_{2x}}{[(\lambda-1)h_1 + h_0]\, p_{2x}} \right\}, \tag{4b}$$

where $p_{1x} = \partial p_1/\partial x$ and $p_{2x} = \partial p_2/\partial x$ are the driving forces, and $\lambda \equiv \mu_2/\mu_1$ denotes the viscosity ratio of the two fluids, as defined at the beginning of this section.

Next, we define the vertically averaged velocities in the two fluids as $\langle u_1 \rangle$ and $\langle u_2 \rangle$,

$$\langle u_1 \rangle(x,t) = \frac{1}{h_1(x,t)} \int_0^{h_1(x,t)} u_1(x,y,t)\, \mathrm{d}y, \tag{5a}$$

$$\langle u_2 \rangle(x,t) = \frac{1}{h_2(x,t)} \int_{h_1(x,t)}^{h_0} u_2(x,y,t)\, \mathrm{d}y. \tag{5b}$$

Then, using (4), we obtain the relationships between the average velocities and the pressure gradients in the horizontal direction,

$$\begin{pmatrix} \langle u_1 \rangle \\ \langle u_2 \rangle \end{pmatrix} = -\frac{1/(12\mu_1)}{(\lambda-1)h_1 + h_0} \begin{pmatrix} h_1^2[4(h_0-h_1) + \lambda h_1] & 3h_1(h_0-h_1)^2 \\ 3(h_0-h_1)h_1^2 & \dfrac{(h_0-h_1)^2}{\lambda}(h_0 - h_1 + 4\lambda h_1) \end{pmatrix} \begin{pmatrix} p_{1x} \\ p_{2x} \end{pmatrix}. \tag{6}$$

For an incompressible steady motion, the conservation of flow rate prescribes that

$$h_1(x,t)\langle u_1 \rangle + (h_0 - h_1(x,t))\, \langle u_2 \rangle = q. \tag{7}$$

Substituting the expressions for the average velocities (6) into Eq. (7), together with Eq. (1), we obtain the pressure gradients corresponding to fluid injection and buoyancy,

$$p_{1x} = -\frac{12\lambda[(\lambda-1)h_1 + h_0]\mu_1 q}{\omega(\lambda,h_0,h_1)} + \frac{\left((\lambda h_1^2 - (h_0-h_1)^2)^2 - \lambda^2 h_1^4 + \lambda h_1(4h_0 + h_1)(h_0-h_1)^2\right)\Delta\rho g \frac{\partial h_1}{\partial x}}{\omega(\lambda,h_0,h_1)}, \tag{8a}$$

$$p_{2x} = -\frac{12\lambda\,[(\lambda-1)h_1 + h_0]\,\mu_1 q + \lambda h_1^2\left(3h_0^2 + h_1[(\lambda-1)h_1 - 2h_0]\right)\Delta\rho g \frac{\partial h_1}{\partial x}}{\omega(\lambda,h_0,h_1)}, \tag{8b}$$

where

$$\omega(\lambda,h_0,h_1) \equiv (\lambda h_1^2 - (h_0-h_1)^2)^2 + 4\lambda h_1(h_0-h_1)h_0^2. \tag{9}$$

From (8), it can be seen that the pressure gradients include two components, i.e., the contributions from fluid injection q and from buoyancy $\Delta\rho g \partial h_1/\partial x$. During the fluid injection process, the fluid-fluid interface $h_1(x,t)$ changes with time; thus, the contribution of fluid injection and buoyancy to the horizontal pressure gradients can change with time.

A. Interface dynamics

The local continuity equation for each fluid layer requires that

$$\frac{\partial h_1}{\partial t} + \frac{\partial}{\partial x}\left(h_1\langle u_1\rangle\right) = 0, \tag{10a}$$

$$\frac{\partial h_2}{\partial t} + \frac{\partial}{\partial x}\left(h_2\langle u_2\rangle\right) = 0. \tag{10b}$$

Incorporating (8) and (6) into the continuity equations (10), we obtain a single nonlinear advection-diffusion equation for the time evolution of the fluid-fluid interface,

$$\frac{\partial h_1}{\partial t} + q\frac{\partial}{\partial x}\left(\frac{\lambda h_1^2\left(3h_0^2 + h_1\left[(\lambda-1)h_1 - 2h_0\right]\right)}{\omega\left(\lambda,h_0,h_1\right)}\right) = \frac{\Delta\rho g}{3\mu_1}\frac{\partial}{\partial x}\left(\frac{h_1^3(h_0-h_1)^3((\lambda-1)h_1+h_0)}{\omega\left(\lambda,h_0,h_1\right)}\frac{\partial h_1}{\partial x}\right). \tag{11}$$

Appropriate initial and boundary conditions are needed to complete the problem. We assume that fluid injection begins at $t=0$, i.e.,

$$h_1(x,0) = 0. \tag{12}$$

Let us denote $x_{f1}(t)$ as the front of the interface that attaches to the top boundary (see Figure 1), i.e., the first boundary condition is given by

$$h_1\left(x_{f1}(t),t\right) = 0. \tag{13}$$

For a constant rate of injection, the constraint of global mass conservation requires that

$$\int_0^{x_{f1}(t)} h_1(x,t)\mathrm{d}x = qt. \tag{14}$$

Equation (11) can be integrated from $x=0$ to $x=x_{f1}(t)$, and then using Eqs. (13) and (14), we obtain a second boundary condition at $x=0$ for $h_1(x,t)$,

$$q\frac{\lambda h_1^2\left(3h_0^2 + h_1\left[(\lambda-1)h_1 - 2h_0\right]\right)}{\omega\left(\lambda,h_0,h_1\right)} - \frac{\Delta\rho g}{3\mu_1}\frac{h_1^3(h_0-h_1)^3((\lambda-1)h_1+h_0)}{\omega\left(\lambda,h_0,h_1\right)}\frac{\partial h_1}{\partial x}\bigg|_{x=0} = q. \tag{15}$$

Note that we have assumed that there is no fluid entrainment at the front of the fluid-fluid interface, i.e., $h_1^3\frac{\partial h_1}{\partial x}\big|_{x=x_{f1}(t)} = 0$.

B. Non-dimensionalization

Let us now rescale the governing equation (11) based on dimensionless variables $H = h_1/h_0$, $X = x/x_c$, $T = t/t_c$, with x_c and t_c chosen as (note $\Delta\rho > 0$)

$$x_c = \frac{\Delta\rho g h_0^4}{\mu_1 q}, \tag{16a}$$

$$t_c = \frac{\Delta\rho g h_0^5}{\mu_1 q^2}. \tag{16b}$$

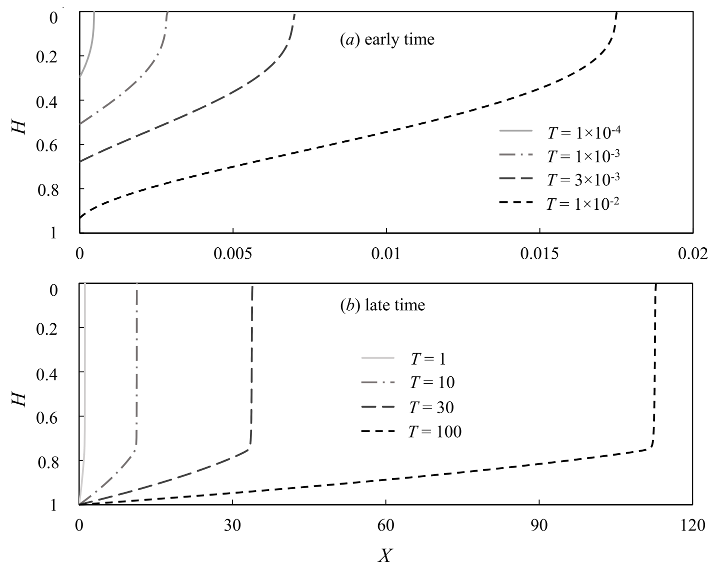

FIG. 2. Typical time evolution of the shape of the fluid-fluid interface from numerical solutions of Eq. (17) subject to (19) with $\lambda = 1$. (a) In the early time period, the fluid interface does not attach to the bottom boundary. (b) In the late time period, the fluid interface attaches to both the top and bottom boundaries.

Then, Eq. (11) in dimensionless form is

$$\frac{\partial H}{\partial T} + \frac{\partial}{\partial X}\left(\frac{\lambda H^2(3 + H[(\lambda-1)H-2])}{\Omega(\lambda,H)}\right) = \frac{1}{3}\frac{\partial}{\partial X}\left(\frac{H^3(1-H)^3((\lambda-1)H+1)}{\Omega(\lambda,H)}\frac{\partial H}{\partial X}\right), \tag{17}$$

where

$$\Omega(\lambda,H) \equiv (\lambda H^2 - (1-H)^2)^2 + 4\lambda H(1-H). \tag{18}$$

The initial and boundary conditions can also be rewritten in dimensionless form,

$$H(X,0) = 0, \tag{19a}$$

$$H\left(X_{f1}(T),T\right) = 0, \tag{19b}$$

$$\frac{\lambda H^2(3 + H[(\lambda-1)H-2])}{\Omega(\lambda,H)} - \frac{1}{3}\frac{H^3(1-H)^3((\lambda-1)H+1)}{\Omega(\lambda,H)}\frac{\partial H}{\partial X}\bigg|_{X=0} = 1, \tag{19c}$$

where $X_{f1}(T) \equiv x_{f1}(t)/x_c$ denotes the location of the front along the top boundary.

Equation (17) along with initial and boundary conditions (19) can be solved numerically and provides the dynamics of the fluid-fluid interface. The equation only involves one parameter λ, which is the viscosity ratio. We employ a central-difference scheme in the numerical study, which is second-order accurate in both time and space.[22,31] We note that the convection-diffusion structure of (17) is characteristic of injection problems with buoyancy driven flows.[21–23] In particular, Taghavi *et al.*[23] studied the same partial differential equation (PDE) with different boundary and initial conditions.

Typical numerical solutions for the dynamics of the interface shape are shown in Figure 2 with $\lambda = 1$ as an example. It can be seen that in the early time period, the fluid interface only attaches to the top boundary, while in the late time period, the interface appears to attach to both the top and bottom boundaries. The numerical solutions motivate us to seek the distinct early and late time asymptotic descriptions. In Sec. III, we provide a well-known self-similar solution as an approximation for the flow behaviour in the early time period; in Sec. IV, we provide another analytical solution to approximate the flow behaviour in the late time period.

III. EARLY TIME BEHAVIOUR

The governing equation (17) contains three terms: an unsteady term, an advective term, and a diffusive term. For this moving boundary problem, there exists no fixed horizontal length scale. The characteristic time and length scales (16) have been chosen such that the advective and the diffusive terms in Eq. (11) have the same order of magnitude at $t = t_c$ when $\lambda = 1$.

In the early time period, i.e., $T \ll 1$, the horizontal length of the current $x \ll x_c$, or equivalently, $X \ll 1$. Equation (17) suggests that the scale of the advective term varies as X^{-1}, while the scale of the diffusive term varies as X^{-2}. Thus, in the early time period, the advective term is negligible compared with the diffusive term. In addition, in the early time period, both $H \ll 1$ and $|(\lambda - 1)H| \ll 1$ hold such that the current is effectively unconfined. Then, the advection-diffusion equation is reduced to a nonlinear diffusion equation, which describes the spreading of a viscous gravity current on an impermeable horizontal substrate,[8]

$$\frac{\partial H}{\partial T} = \frac{1}{3}\frac{\partial}{\partial X}\left(H^3\frac{\partial H}{\partial X}\right). \tag{20}$$

The global mass conservation equation in dimensionless form gives

$$\int_0^{X_f(T)} H(X,T)\mathrm{d}X = T. \tag{21}$$

Equations (20) and (21) and boundary condition (19b) admit a self-similar solution, which is well known.[8]

To construct this self-similar solution, we first define an appropriate similarity variable $\xi \equiv 3^{1/5}X/T^{4/5}$; thus, the front propagates as $X_{f1}(T) = \xi_f T^{4/5}/3^{1/5}$, where ξ_f is a constant to be determined. We then introduce $s \equiv X/X_{f1}(T) = \xi(X,T)/\xi_f$, so that the shape of the interface can be expressed in the generalized self-similar form $H(X,T) = \xi_f^{2/3}3^{1/5}T^{1/5}f(s)$. Here, $f(s)$ and ξ_f are the solutions to the system,

$$(f^3f')' + \frac{4}{5}sf' - \frac{1}{5}f = 0, \tag{22a}$$

$$f(1) = 0, \tag{22b}$$

$$\xi_f = \left(\int_0^1 f(s)\,\mathrm{d}s\right)^{-3/5}, \tag{22c}$$

with the primes denoting differentiation with respect to s. We can determine the asymptotic behaviour near the front of the interface based on Eqs. (22a) and (22b),

$$f(s) \sim \left(\frac{12}{5}\right)^{\frac{1}{3}}(1-s)^{\frac{1}{3}} \quad \text{as } s \to 1^-. \tag{23}$$

Equation (23) provides two boundary conditions near the front $s = 1$, i.e., $f(1-\epsilon)$ and $f'(1-\epsilon)$ with $\epsilon \ll 1$, which can be used in a shooting procedure for numerically solving Eq. (22a). The value of the pre-factor in the similarity solution for $H(X,T)$ is calculated numerically as $\xi_f \approx 1.0$. Thus, we have obtained a self-similar solution for the nonlinear diffusion problem, and the front that attaches to the top boundary propagates as $X_{f1}(T) \approx 0.8T^{4/5}$. The numerically computed shape $f(s)$ is shown in Figure 3.

Thus, in the early time period, the shape of the interface is described by the self-similar solution to Eq. (20) subject to the global mass constraint (21). In Figure 4, this solution is plotted along with numerical solutions of the advection-diffusion equation (17) with boundary and initial conditions (19). $H_f(T)$ represents the location of the vertical front along H axis in Figure 4, and the numerical solution agrees well with the similarity solution from (22) in the early time period. As time increases, the numerical solutions depart from the similarity solution. In addition, the early-time self-similar solution holds longer when λ decreases; a more detailed analysis on the transition time scale is provided in Sec. V.

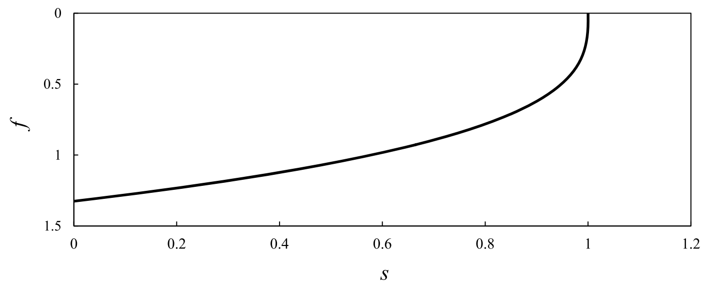

FIG. 3. Early time self-similar solution to the nonlinear diffusion equation (20) subject to the global mass constraint (21). Using an appropriate similarity transform, the corresponding ordinary differential equation (ODE) and boundary conditions are given by Eq. (22). This early time result is well known, highlights the unconfined character of the early time solution, and breaks down somewhat before the current attaches to the bottom boundary.

IV. LATE TIME BEHAVIOUR

We next consider (17) at long times when the convective term can no longer be neglected. We treat separately $\lambda = 1$ and $\lambda \neq 1$. The basic structure of this late time analysis has similarity with Taghavi *et al.*[23] though some more analytical results are obtained below.

A. Equal viscosities: $\lambda = 1$

Let us start from the special case of $\lambda = 1$, i.e., when the injected and displaced fluids have equal viscosities. The governing equation (17) reduces to

$$\frac{\partial H}{\partial T} + \frac{\partial}{\partial X}\left(H^2(3-2H)\right) = \frac{1}{3}\frac{\partial}{\partial X}\left(H^3(1-H)^3\frac{\partial H}{\partial X}\right). \tag{24}$$

In the late time period, the interface attaches to both the top and bottom boundaries, as can be verified numerically, and we denote the front location at the top (bottom) boundary by $X_{f1}(T)$ ($X_{f2}(T)$) with $X_{f1}(T) > X_{f2}(T) \geq 0$ since the top front moves faster. Again, Eq. (24) suggests that the scale of the advective term $\propto X^{-1}$, while the scale of the diffusive term $\propto X^{-2}$. Thus, we neglect the diffusive term in the late time period when $X \gg 1$, and the full governing equation (24) is approximated by a nonlinear hyperbolic equation,

$$\frac{\partial H}{\partial T} + \frac{\partial}{\partial X}\left(H^2(3-2H)\right) = 0. \tag{25}$$

The front conditions are given by

$$H\left(X_{f1}(T), T\right) = 0, \tag{26a}$$

$$H\left(X_{f2}(T), T\right) = 1. \tag{26b}$$

Now, we seek a self-similar solution for Eq. (25) subject to (26). It should be noted that an initial condition is not necessary since we are seeking a self-similar solution for long times. The initial condition will eventually be "forgotten," and the (stable) self-similar solution we obtain is considered an intermediate asymptotic behaviour.[2]

For Eq. (25), we denote the convective flux function as $F(H) \equiv H^2(3-2H)$, which is neither convex nor concave. We define a similarity variable as $\xi = X/T$. After some manipulation, Eq. (25) reduces to

$$\frac{\mathrm{d}H}{\mathrm{d}\xi}\left(\frac{\mathrm{d}F}{\mathrm{d}H} - \xi\right) = 0. \tag{27}$$

Solving $\mathrm{d}H/\mathrm{d}\xi = 0$ provides a trivial solution. Thus, we solve $\mathrm{d}F/\mathrm{d}H = \xi$, which can be rewritten as the algebraic equation,

$$6H(1-H) = \xi. \tag{28}$$

An analytical expression for this quadratic equation is obvious, but it does not satisfy the entropy condition. Thus, we construct a weak solution, i.e., a compound wave solution, which contains a

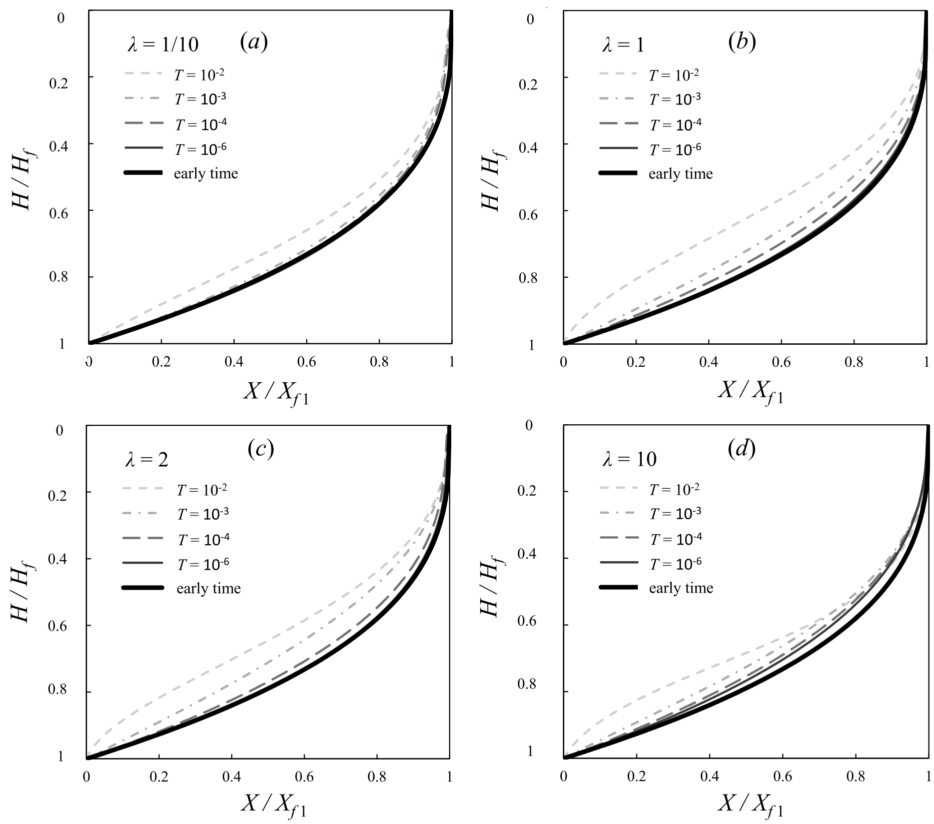

FIG. 4. Time evolution of the fluid-fluid interface in the early time period for different values of λ. (a) $\lambda = 1/10$, (b) $\lambda = 1$, (c) $\lambda = 2$, (d) $\lambda = 10$. The self-similar solution of the nonlinear diffusion equation (22) is also plotted (labeled "early time"), which is independent of the viscosity ratio λ. This self-similar solution agrees well with numerical solutions in the early time period. As time progresses, numerical solutions depart from the self-similar solution.

shock front and a stretching region, by inserting a shock front at a proper location $X_{f1}(T)$, using the "equal-area rule."[32] The compound wave solution to Eq. (28) can be expressed as

$$H(X,T) = \begin{cases} \left(1+\sqrt{1-2X/(3T)}\right)/2, & 0 \le X/T \le 9/8, \\ 0, & X/T > 9/8, \end{cases} \tag{29}$$

which is shown in Figure 5(a). The location of the shock front is $X_{f1}(T) = 9T/8$, and the height of the shock is $H_s = 3/4$. The location of the front that attaches to the bottom boundary is always zero, i.e., $X_{f2}(T) = 0$, because the characteristic speed $\mathrm{d}F/\mathrm{d}H \to 0^+$ as $H \to 1^-$.

B. Different viscosities: $\lambda \neq 1$

Let us now consider the effect of the viscosity ratio on the solutions in the late time period. The viscosity ratio is defined as $\lambda \equiv \mu_2/\mu_1$, where μ_1 denotes the viscosity of the injected less dense fluid and μ_2 denotes the viscosity of the denser fluid. In the late time period, by neglecting the diffusive term, the full governing equation (17) is approximated by the nonlinear hyperbolic equation,

$$\frac{\partial H}{\partial T} + \frac{\partial}{\partial X}\left(\frac{\lambda H^2(3+H((\lambda-1)H-2))}{(\lambda H^2-(1-H)^2)^2+4\lambda H(1-H)}\right) = 0. \tag{30}$$

Let us denote the convective flux function by

$$F(H) = \frac{\lambda H^2(3+H((\lambda-1)H-2))}{(\lambda H^2-(1-H)^2)^2+4\lambda H(1-H)}, \tag{31}$$

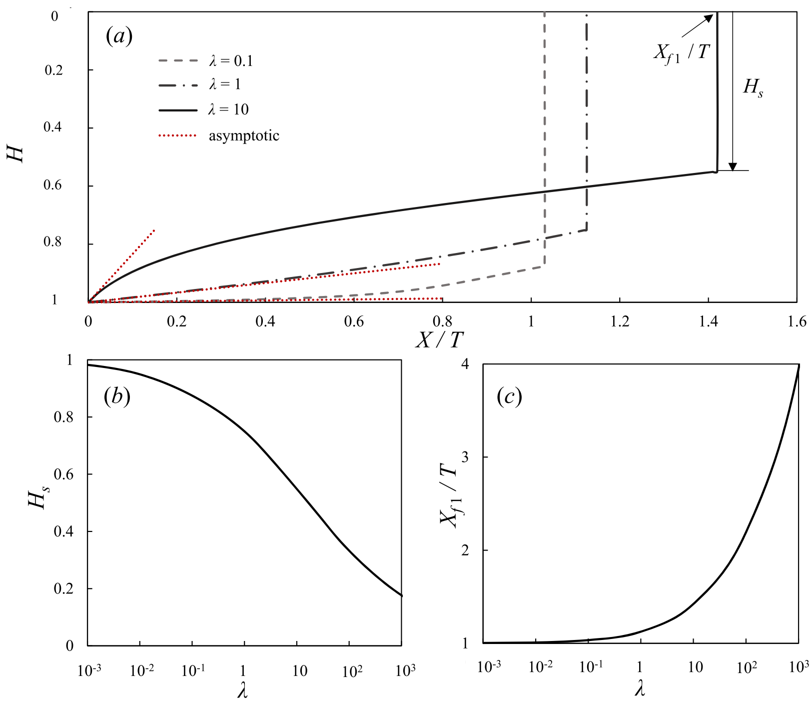

FIG. 5. (a) Late time compound wave solutions of the nonlinear hyperbolic equation (30) for different values of λ, and the asymptotic behaviour as $H \to 1^-$ based on Eq. (34). (b) and (c) The influence of viscosity ratio λ on (b) the height of the shock H_s and (c) the location of the front X_{f1}/T.

and hence, the characteristic speed is

$$\frac{\mathrm{d}F}{\mathrm{d}H} = \frac{6\lambda H(H-1)\left((\lambda-1)^2H^4 - 2(\lambda-1)^2H^3 - 2(\lambda-1)H - 1\right)}{\left((\lambda-1)^2H^4 + 4(\lambda-1)H^3 - 6(\lambda-1)H^2 + 4(\lambda-1)H + 1\right)^2}. \tag{32}$$

Again, we define a similarity variable $\xi = X/T$, we find (27), and we seek solutions to $\mathrm{d}F/\mathrm{d}H = \xi$. Note that the flux function (31) is neither concave nor convex; thus, again, we construct a compound wave solution $H(\xi)$ to describe the time evolution of the fluid-fluid interface using the "equal-area" rule.[32] The compound wave solutions corresponding to different values of λ are calculated numerically and shown in Figure 5(a) with $\lambda = 1/10, 1,$ and 10 as examples. The influence of viscosity ratio on the height of the shock H_s and the location of the shock front $X_{f1}(T)$ is provided, respectively, in Figures 5(b) and 5(c).

The asymptotic behaviour as $H \to 1^-$, when the current attaches to the boundary, can also be studied. Let us denote $H = 1 - \delta$ with $\delta \to 0^+$ as $H \to 1^-$, and (32) can be expanded in power series,

$$\lim_{H\to 1^-} \frac{\mathrm{d}F}{\mathrm{d}H} = \frac{6\delta}{\lambda} + \frac{6(5\lambda-6)\delta^2}{\lambda^2} + O\left(\delta^3\right). \tag{33}$$

Thus, the leading-order asymptotic solution as $H \to 1^-$ can be obtained as a linear function of the similarity variable,

$$H(X,T) \sim 1 - \frac{\lambda}{6}\frac{X}{T} \quad \text{as } H \to 1^-, \tag{34}$$

which is also shown in Figure 5(a) for $\lambda = 1/10, 1,$ and 10 as examples.

In addition, we can keep both the first and second order terms in Eq. (33); together with $\mathrm{d}F/\mathrm{d}H = \xi$, we obtain

$$\lim_{\delta\to 0^+} \frac{\mathrm{d}^2\delta}{\mathrm{d}\xi^2} = \frac{12-10\lambda}{\lambda}\left(\frac{\mathrm{d}\delta}{\mathrm{d}\xi}\right)^2, \tag{35}$$

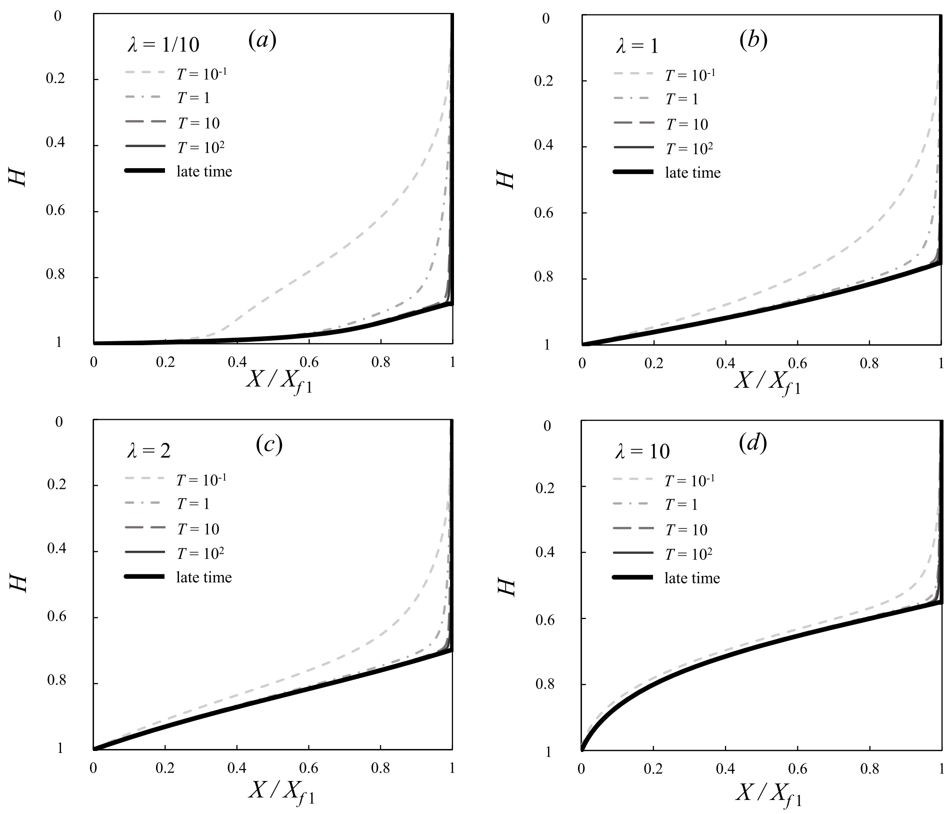

FIG. 6. Time evolution of the fluid-fluid interface according to Eq. (17) in the late time period for different values of λ. (a) $\lambda = 1/10$, (b) $\lambda = 1$, (c) $\lambda = 2$, (d) $\lambda = 10$. The compound wave solution of the nonlinear hyperbolic equation (30) is also plotted. Numerical solutions approach the compound wave solution in the late time period of the simulation.

and

$$\lim_{H \to 1^-} \frac{\mathrm{d}^2 H}{\mathrm{d}\xi^2} = \begin{cases} -12\lambda^{-1}(\mathrm{d}H/\mathrm{d}\xi)^2, & \lambda \ll 1, \\ 10(\mathrm{d}H/\mathrm{d}\xi)^2, & \lambda \gg 1, \end{cases} \tag{36}$$

which represents the concavity of the interface in Figure 5(a) as $\delta \to 0^+$, i.e., $H \to 1^-$. The concavity depends on the value of the viscosity ratio λ, with a crossover at $\lambda = 6/5$. In particular, for $\lambda \ll 1$, we have $\mathrm{d}^2H/\mathrm{d}\xi^2 < 0$; however, for $\lambda \gg 1$, we obtain $\mathrm{d}^2H/\mathrm{d}\xi^2 > 0$. The results are consistent with the observations in Figure 5(a).

In summary, in the late time period, we neglect the diffusive term in Eq. (17), and we obtain nonlinear hyperbolic equation (25) or (30) to describe the time evolution of the fluid-fluid interface. Since the flux function is neither convex nor concave, we can construct a compound wave solution to the nonlinear hyperbolic equation, for example, solution (29) to Eq. (25) for $\lambda = 1$. The height of the shock H_s and the location of the shock front $X_{f1}(T)$ depend on the viscosity ratio λ (see Figures 5(b) and 5(c)). Various compound wave solutions for different values of λ are plotted along with numerical solutions to the full equation (17) at different times with boundary and initial conditions given by (19), see in Figure 6. The numerical solutions approach the compound wave solutions in the late time period.

V. TRANSITION PROCESSES

A. Front propagation laws

To demonstrate the transition processes between the short time and long time behaviours described in Secs. III and IV, respectively, we track the locations of the propagating front $X_{f1}(T)$ that

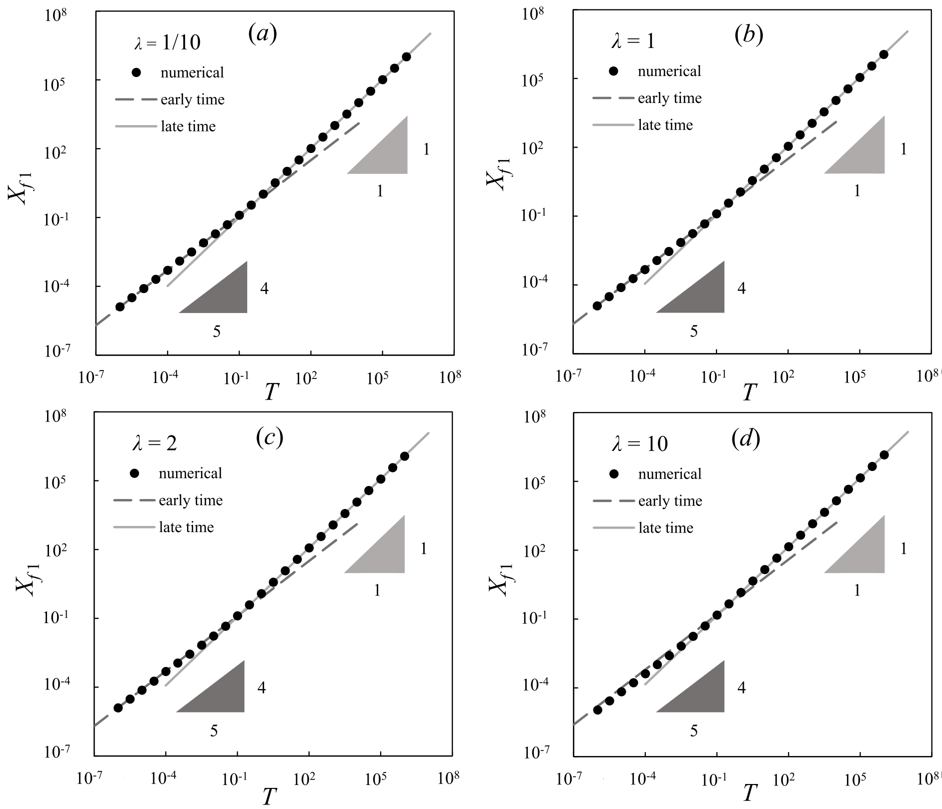

FIG. 7. Time evolution of the location of the propagating front for different values of λ: transition from an early time self-similar behaviour to a late time self-similar behaviour. (a) $\lambda = 1/10$, (b) $\lambda = 1$, (c) $\lambda = 2$, (d) $\lambda = 10$. The front locations are obtained from the numerical solution of Eq. (17). In the early time period, the front propagates obeying a power law form $X_{f1}(T) \propto T^{4/5}$; in the late time period, the front propagates linearly, i.e., $X_{f1}(T) \propto T$.

attaches to the top boundary at various times, where $H(X_{f1}(T), T) = 0$. In the early time period, the interface spreads obeying the nonlinear diffusion equation (20) subject to the global mass constraint (21), and the front propagates in the power law form $X_{f1}(T) \propto T^{4/5}$. In the late time period, the interface shape is governed by the nonlinear hyperbolic equation (30), and the front moves linearly: $X_{f1}(T) \propto T$. The transition from the early to the late time behaviour is shown in Figure 7 with $\lambda = 1/10, 1, 2$, and 10 as examples. The predictions of the front locations from numerical solutions to the full equation (17) are shown as dots, while the predictions from the various approximate solutions are plotted as the dashed line (early time) and solid line (late time).

B. Injection regimes

The dynamics of fluid injection into a two-dimensional horizontal confined channel can be summarized in a regime diagram, shown in Figure 8, with regard to two dimensionless groups: the viscosity ratio λ and the dimensionless time T. We have obtained three distinct dynamic regimes: a nonlinear diffusion regime (I), a transition regime (II), and a hyperbolic regime (III). In regime I, the dynamics of the interface corresponds to the early time behaviour described in Sec. III; in regime III, the dynamics of the interface follows the late time behaviour described in Sec. IV.

The boundaries distinguishing each regimes (the dashed curves) are defined as the crossover time when the location of the top front has a 10% difference between the predictions of the numerical and self-similar solutions in the early and late time periods. For $\lambda \gg 1$, the slope of the boundary between regimes II and III is approximately 5, which corresponds to the requirement to reduce the

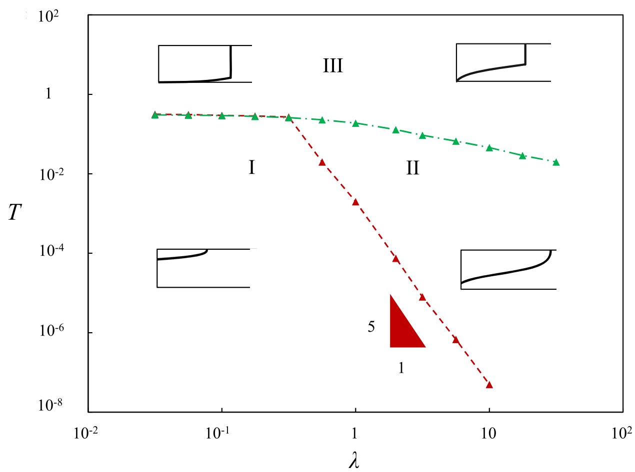

FIG. 8. Flow regime for fluid injection into a two-dimensional channel with regard to two dimensionless groups: viscosity ratio λ and dimensionless time T. The symbols and dashed curves indicate the time when the location of the top front has a 10% difference between the predictions of the numerical solution to the full governing equation (17) and the self-similar solutions in the early and late time periods. In regime I, the self-similar solution from the nonlinear diffusion equation corresponding to the early time behaviour gives a good estimate, while in regime III, the compound wave solution corresponding to the late time behaviour provides a good approximation. Regime II is the transition regime, where a numerical solution of the full equation is necessary to provide the time evolution of the fluid-fluid interface.

full equation (17) to the nonlinear diffusion equation (20) in the early time period: $(\lambda - 1)H \ll 1$, or $\lambda T^{1/5} \ll 1$ with $\lambda \gg 1$, based on the results in Sec. III.

VI. FINAL REMARKS

A. Summary and conclusions

We have studied the dynamics of fluid injection into a two-dimensional confined channel filled with another fluid of different density and viscosity. Such flows may occur during various cleaning or displacement operations, for example. Neglecting the mixing and the interfacial tension between the two fluids, and assuming a distance of propagation long compared to the channel height, the incompressible form of Stokes equations reduces to nonlinear advection-diffusion equation (11) that describes the time evolution of the fluid-fluid interface.

We studied the governing equation analytically and identified different behaviours in the early and late time periods. Specifically, in the early time period, the advection-diffusion equation reduces to nonlinear diffusion equation (20), and a self-similar solution is obtained;[10] in the late time period, the advection-diffusion equation has been approximated by hyperbolic equation (30), and a compound wave solution is obtained to describe the dynamics of the fluid-fluid interface.[23] We have also numerically solved the dimensionless advection-diffusion equation (17) with appropriate boundary and initial conditions (19). The numerical solutions agree well with the distinct analytical solutions in both the early and late time periods. Finally, we summarized these ideas in a regime diagram, which gives the flow behaviour with regard to two dimensionless groups: the viscosity ratio λ and the dimensionless time T; and three different dynamical regimes are identified in the diagram: a nonlinear diffusion regime, a hyperbolic regime, and a transition regime.

B. Exchange flow with injection

In this paper, we have assumed that fluid injection started at $t = 0$ from the origin of the system. Therefore, the displaced fluid occupies the entire channel before fluid injection occurs. There exists another related flow system: the viscous exchange flow generated by removing a lock gate between two fluids of different density and viscosity.[23,29] For viscous exchange flow, when one fluid is imposed with a constant injection rate, the same advection-diffusion equation (17) describes the time evolution of the fluid-fluid interface in a horizontal channel. However, the boundary and initial conditions are different, compared with the injection problem investigated in this paper. In addition, the global mass conservation equation (14) no longer holds, and hence the early time behaviour for exchange flow system with constant injection is different from the self-similar behaviour described in Sec. III. However, in the late time period, the compound wave solution, described in Sec. IV, can still be used as a good approximation for the dynamics of the free interface.

C. Wide channel versus narrow channel

In this paper, we study flow in a two-dimensional channel, which corresponds to a channel with width w much greater than depth h_0, i.e., $w \gg h_0$. Thus, the drag from the side walls has not been considered in deriving the velocity field (4), and we have only considered the drag from the top and bottom boundaries. However, when the channel width is much smaller than the depth, i.e., $w \ll h_0$, the drag from the side walls becomes important compared with the drag from the top and bottom boundaries. In that case, the governing equation for the dynamics of the fluid-fluid interface is equivalent to the equation governing fluid injection into a confined porous medium (with porosity $\phi = 1$ and permeability $k = w^2/12$), which has been previously studied.[12,21,22] Compared with our paper, the time evolution of the fluid-fluid interface behaves differently in both the early and late time periods: the interface obeys a different nonlinear diffusion behaviour in the early time period; in the late time period, the dynamics of the interface can be described by three distinct self-similar solutions, depending on the viscosity ratio.[21,22]

D. Saffman-Taylor instability

It should be noted that with $\lambda > 1$, i.e., the injected fluid is less viscous than the displaced fluid, and the flow situation corresponds to the condition when the Saffman-Taylor instability occurs.[33,34] Our model assumes that the shape of the fluid-fluid interface is monotonic because of the buoyancy effect, and we obtain a compound wave solution to describe the time evolution of the fluid-fluid interface. A similar situation also exists for the flow during fluid injection into a confined porous medium initially saturated with another fluid of different density and larger viscosity.[21,22] For example, Pegler *et al*.[21] conducted experiments in Hele-Shaw cells filled with glass beads and observed that the Saffman-Taylor instability does not occur at the reservoir scale, and the theoretical predictions provide good approximations to the fluid-fluid interface except in the region close to the propagating front. The suppression of the Saffman-Taylor instability is possibly due to the vertical pressure gradient from the hydrostatic pressure distribution, and it remains an interesting problem for future investigation.

ACKNOWLEDGMENTS

We are grateful for a grant from the Princeton Carbon Mitigation Initiative for support of this research. L.R. thanks the Fonds Alfred Renard and the Belgian American Educational Foundation for financial support. We also thank I. C. Christov, B. Guo, A. Hogg, and R. H. Socolow for helpful discussions.

1 J. Bear, *Dynamics of Fluids in Porous Media* (Elsevier, 1972).
2 G. I. Barenblatt, *Similarity, Self-Similarity, and Intermediate Asymptotics* (Consultants Bureau, 1979).
3 L. W. Lake, *Enhanced Oil Recovery* (Prentice Hall, 1989).
4 J. M. Nordbotten and M. A. Celia, *Geological Storage of* CO_2 (John Wiley & Sons, Inc., 2012).
5 H. E. Huppert and J. A. Neufeld, "The fluid mechanics of carbon dioxide sequestration," Annu. Rev. Fluid Mech. **46**, 255–272 (2014).
6 S. H. Smith, "On initial value problems for the flow in a thin sheet of viscous liquid," ZAMP **20**, 556–560 (1969).
7 N. Didden and T. Maxworthy, "The viscous spreading of plane and axisymmetric gravity currents," J. Fluid Mech. **121**, 27–42 (1982).
8 H. E. Huppert, "The propagation of two-dimensional and axisymmetric viscous gravity currents over a rigid horizontal surface," J. Fluid Mech. **121**, 43–58 (1982).
9 J. Gratton and F. Minotti, "Self-similar viscous gravity currents: Phase plane formalism," J. Fluid Mech. **210**, 155–182 (1990).

[10] H. E. Huppert, "Flow and instability of a viscous current down a slope," Nature **300**, 427–429 (1982).
[11] J. R. Lister, "Viscous flows down an inclined plane from point and line sources," J. Fluid Mech. **242**, 631–653 (1992).
[12] H. E. Huppert and A. W. Woods, "Gravity driven flows in porous layers," J. Fluid Mech. **292**, 55–69 (1995).
[13] J. M. Acton, H. E. Huppert, and M. G. Worster, "Two-dimensional viscous gravity currents flowing over a deep porous medium," J. Fluid Mech. **440**, 359–380 (2001).
[14] S. Lyle, H. E. Huppert, M. Hallworth, M. Bickle, and A. Chadwick, "Axisymmetric gravity currents in a porous medium," J. Fluid Mech. **543**, 293–302 (2005).
[15] V. Mitchell and A. W. Woods, "Self-similar dynamics of liquid injected into partially saturated aquifers," J. Fluid Mech. **566**, 345–355 (2006).
[16] Z. Zheng, I. C. Christov, and H. A. Stone, "Influence of heterogeneity on second-kind self-similar solutions for viscous gravity currents," J. Fluid Mech. **747**, 218–246 (2014).
[17] D. Takagi and H. E. Huppert, "The effect of confining boundaries on viscous gravity currents," J. Fluid Mech. **577**, 495–505 (2007).
[18] Z. Zheng, B. Soh, H. E. Huppert, and H. A. Stone, "Fluid drainage from the edge of a porous reservoir," J. Fluid Mech. **718**, 558–568 (2013).
[19] M. A. Hesse, H. A. Tchelepi, B. J. Cantwell, and F. M. Orr, Jr., "Gravity currents in horizontal porous layers: Transition from early to late self-similarity," J. Fluid Mech. **577**, 363–383 (2007).
[20] Y. Hallez and J. Magnaudet, "A numerical investigation of horizontal viscous gravity currents," J. Fluid Mech. **630**, 71–91 (2009).
[21] S. S. Pegler, H. E. Huppert, and J. A. Neufeld, "Fluid injection into a confined porous layer," J. Fluid Mech. **745**, 592–620 (2014).
[22] Z. Zheng, B. Guo, I. C. Christov, M. A. Celia, and H. A. Stone, "Flow regimes for fluid injection into a confined porous medium," J. Fluid Mech. **767**, 881–909 (2015).
[23] S. M. Taghavi, D. M. Martinez, and I. A. Frigaard, "Buoyancy-dominated displacement flows in near-horizontal channels: The viscous limit," J. Fluid Mech. **639**, 1–35 (2009).
[24] J. M. Nordbotten and M. A. Celia, "Similarity solutions for fluid injection into confined aquifers," J. Fluid Mech. **561**, 307–327 (2006).
[25] M. A. Hesse, F. M. Orr, Jr., and H. A. Tchelepi, "Gravity currents with residual trapping," J. Fluid Mech. **611**, 35–60 (2008).
[26] C. W. MacMinn, M. L. Szulczewski, and R. Juanes, "CO_2 migration in saline aquifers. Part 1. Capillary trapping under slope and groundwater flow," J. Fluid Mech. **662**, 329–351 (2010).
[27] C. W. MacMinn, M. L. Szulczewski, and R. Juanes, "CO_2 migration in saline aquifers. Part 2. Combined capillary and solubility trapping," J. Fluid Mech. **688**, 321–351 (2011).
[28] I. Gunn and A. W. Woods, "On the flow of buoyant fluid injected into a confined, inclined aquifer," J. Fluid Mech. **672**, 109–129 (2011).
[29] G. P. Matson and A. J. Hogg, "Viscous exchange flows," Phys. Fluids **24**, 023102 (2012).
[30] S. Saha, D. Salin, and L. Talon, "Low Reynolds number suspension gravity currents," Eur. Phys. J. E **36**, 10385 (2013).
[31] A. Kurganov and E. Tadmor, "New high-resolution central schemes for nonlinear conservation laws and convection-diffusion equations," J. Comput. Phys. **160**, 241–282 (2000).
[32] R. J. LeVeque, *Finite Volume Methods for Hyperbolic Problems* (Cambridge University Press, 2002).
[33] P. G. Saffman and G. I. Taylor, "The penetration of a fluid into a porous medium or Hele-Shaw cell containing a more viscous liquid," Proc. R. Soc. A **245**, 312–329 (1958).
[34] G. M. Homsy, "Viscous fingering in porous media," Annu. Rev. Fluid Mech. **19**, 271–311 (1987).